Network-Based Analysis on Orthogonal Separation of Human Plasma Uncovers Distinct High Density Lipoprotein Complexes

Hailong Li,[§,†] Scott M. Gordon,[‡] Xiaoting Zhu,[†] Jingyuan Deng,[†] Debi K. Swertfeger,[†] W. Sean Davidson,[‡] and L. Jason Lu*[,†]

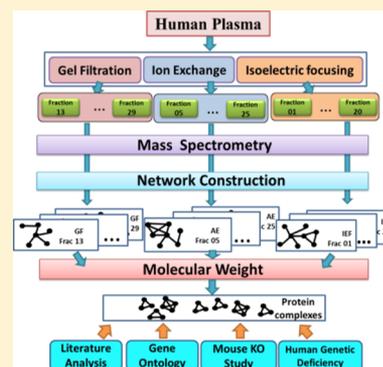[§]Institute for Systems Biology, Jianghan University, Wuhan, Hubei, 430056, P.R. China

[†]Division of Biomedical Informatics, Cincinnati Children's Hospital Research Foundation, 3333 Burnet Avenue, MLC 7024, Cincinnati, Ohio 45229-3039, United States

[‡]Center for Lipid and Arteriosclerosis Science, Department of Pathology and Laboratory Medicine, University of Cincinnati, 2120 East Galbraith Road, Cincinnati, Ohio 45237-0507, United States

Ⓢ *Supporting Information*

ABSTRACT: High density lipoprotein (HDL) particles are blood-borne complexes whose plasma levels have been associated with protection from cardiovascular disease (CVD). Recent studies have demonstrated the existence of distinct HDL subspecies; however, these have been difficult to isolate and characterize biochemically. Here, we present the first report that employs a network-based approach to systematically infer HDL subspecies. Healthy human plasma was separated into 58 fractions using our previously published three orthogonal chromatography techniques. Similar local migration patterns among HDL proteins were captured with a novel similarity score, and individual comigration networks were constructed for each fraction. By employing a graph mining algorithm, we identified 183 overlapped cliques, among which 38 were further selected as candidate HDL subparticles. Each of these 38 subparticles had at least two literature supports. In addition, GO function enrichment analysis showed that they were enriched with fundamental biological and CVD protective functions. Furthermore, gene knockout experiments in mouse model supported the validity of these subparticles related to three apolipoproteins. Finally, analysis of an apoA-I deficient human patient's plasma provided additional support for apoA-I related complexes. Further biochemical characterization of these putative subspecies may facilitate the mechanistic research of CVD and guide targeted therapeutics aimed at its mitigation.

KEYWORDS: high-density lipoprotein, proteomics, protein network, comigration pattern, subspecies, apolipoprotein, maximal clique, human plasma, particle fractionation
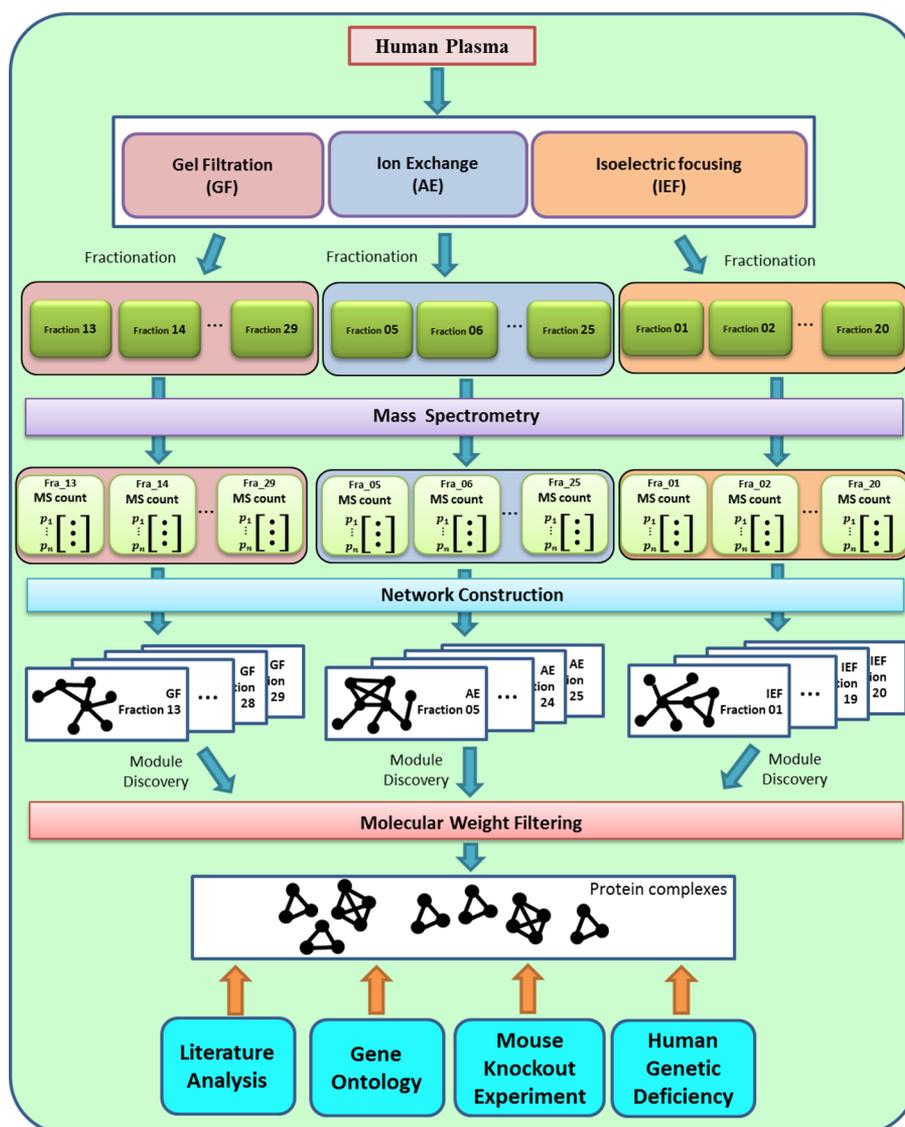

INTRODUCTION

Plasma high density lipoprotein (HDL) is a highly heterogeneous family of particles that ranges from 7−13 nm in diameter. It is composed of proteins and lipids in approximately equal mass. HDL has been epidemiologically associated with protection from atherosclerotic cardiovascular disease (CVD), a leading cause of mortality around the world.[1,2] Recent proteomics studies have identified upward of 89 distinct HDL-associated proteins.[3−11] Among them, roughly 70% of the protein mass consists of apolipoprotein (apo)A-I, and another 15−20% is apoA-II. These major HDL proteins form stable complexes with phospholipids, cholesterol, triglycerides, and cholesteryl esters. The remaining proteins include other classical apolipoproteins[12] such as apoC-II, C−III, E, D, M, and A-IV as well as enzymes, transfer proteins, protease inhibitors, complement factors, and even vitamin-binding proteins.[13]

Plasma HDL cholesterol (HDL-C) level is a well-known negative risk factor for the development of CVD. A widely accepted basis for the inverse relationship between human plasma HDL-C and CVD is the ability of HDL, and its major protein constituent apoA-I, to mediate reverse cholesterol transport (RCT).[14] In this process, HDL promotes cholesterol efflux from peripheral cells such as macrophage-derived foam cells in the vessel wall to transport excess cholesterol and other lipids back to the liver for catabolism. Aside from lipid-transport activities, recent studies have identified an array of additional functions that likely contribute to HDL-mediated cardiovascular protection. For example, HDL has been documented to prevent oxidative modification of LDL via the HDL-associated protein paraoxonase1 (PON1).[15] Another well recognized HDL function is its role as an anti-inflammatory regulator that may slow atherosclerosis progression.[16−18] Additionally, HDL can modulate vascular tone by affecting the production of nitric oxide (NO), a key mediator of vascular smooth muscle cell contraction.[19] These antioxidative, anti-inflammatory, and provasodilatory properties of HDL might have equal

Figure 1. Schematic diagram of the systematic approach to identify HDL complexes based on three orthogonal chromatographic separation techniques. Healthy human plasmas were separated by three separation methods into an array of fractions. For each fraction, MS analysis was performed to discover the identities and spectral counts of proteins. On the basis of abundance profiles, individual comigration networks were constructed with our local S-score. A graph mining algorithm was applied to discover protein complexes. After filtration with molecular weight threshold, multiple validation approaches were utilized to test the putative HDL subspecies.

importance as its well-known cholesterol efflux function in the process of protecting against the CVD development.

Recent studies have demonstrated the existence of distinct HDL subspecies that are defined by unique protein complements. Asztalos et al. used antibodies to visualize individual protein migration patterns in a native 2D gel electrophoresis system and found apoA-I in 11 distinct spots representing variously charged and sized species.[20] In our previous research, we separated human lipoproteins into five individual fractions by ultracentrifugation[7] and 17 fractions by size exclusion chromatography[8] and again saw highly distinct distribution patterns for individual proteins. Additionally, there is emerging evidence that distinct protein particle compositions can result in defined and unexpected functions. The most impressive example to date is the HDL particle dubbed trypanosome lytic factor (TLF).[21,22] This particle contains apoA-I, haptoglobin-related protein (HPR), and apoL-I and has been shown to have specific lytic activity against the protozoan *Trypanosoma brucei*.

This activity is absolutely dependent on the presence of these proteins. Given the widely diverse functions of the HDL-associated proteins and the fact that HDL's CVD protection is mediated through similarly diverse functions, it is reasonable to believe that many of these subspecies may play unique biological roles.

Unfortunately, our knowledge of the structure and functions of HDL subspecies is limited. So far, no existing method can directly reveal the composition of distinct HDL subspecies. Density gradient ultracentrifugation (UC) is currently the preferred method of HDL isolation because density is a major resolving factor between nonlipid and lipid-bound proteins. The underlying principle of this method is to quantitatively float the relatively light lipid-bound proteins away from the heavy nonlipid associated proteins. However, this method often involves prolonged, high speed centrifugation steps and the use of high salt concentrations, which can modify the protein structure and deplete apolipoproteins from the final isolates. In

addition, the high salt must also be removed for further analysis of lipoprotein fractions, a process that results in poor recoveries.[23] Furthermore, Van't Hooft et al. have shown that more than a half of apoE was disassociated with HDL proteins during UC.[24] All of these issues can interfere with our ability to identify specific protein−protein interactions (PPIs) on lipoprotein particles. Thus, there is an urgent need to analyze the HDL proteome using alternative separation techniques.

In our previous study, we applied three novel, nondensity based, orthogonal chromatographic separation techniques on human plasma to better characterize the structural composition and functions of HDL subspecies.[9] These techniques were used to fractionate normal human plasma into phospholipid-containing fractions, and the identities of the proteins were determined using mass spectrometry (MS). The spectral counts obtained from MS analysis of those fractions correlated well with protein abundance as determined by immunological analyses.[7] As such, the distribution of each protein across all the fractions, that is, a migration pattern, was obtained. Our previous work clearly established that certain HDL proteins could comigrate across the separation methodologies, suggesting the existence of discrete subspecies. However, our initial comigration analysis was limited in that it only inferred static interactions by considering global distribution similarity between HDL proteins, which may not effectively reflect the diversity of compositions for distinct HDL subspecies. Moreover, one global protein network was constructed based on those static PPIs using the conventional strategy, similar to several previous large-scale proteomics studies.[25−28] This single-network strategy is certainly beneficial to either uncover important principles of global protein organization or reveal novel protein interactions and complexes. However, it simply assumes spatial−temporal coexistence among nearby network nodes and edges (proteins and interactions) so that one identified protein complex may involve multiple smaller protein complexes in reality. Indeed, in our static protein interaction network, while certain subnetworks were clearly identifiable, the majority of the proteins clustered into one single subnetwork, which limited the utility of the data. Customized network construction strategies and profound graph mining algorithms are crucial for further investigation of HDL subspecies.

In this work, we developed a novel multinetwork based computational approach to systematically identify structural HDL subspecies (Figure 1). The organization of this article is as follows. First, we described the proteomics data upon which our analysis was based followed by the novel scoring system that quantitatively measured the similarity between two given proteins' local distribution patterns. Next, we constructed individual local comigration networks for all fractions and searched the HDL complex candidates in those networks. Finally, we tested those identified candidates using distinct experimental and computational approaches including literature search analysis and Gene Ontology (GO) functional enrichment analysis, a mouse HDL study, and a human genetic disease study.

■ MATERIAL AND METHODS

Lipid-Associated Proteins Distribution Patterns Data Set from Three Orthogonal Separation Chromatography Techniques

We developed three nondensity based orthogonal separation chromatography techniques to fractionate normal human plasma to phospholipid-containing fractions:[9] gel filtration (GF) chromatography that separates particles by molecular size; anion exchange (AE) chromatography that separates particles by charge; and isoelectric focusing (IEF) chromatography that separates particles based on the isoelectric point or the pH at which a particle has a net charge of zero. Considering the completeness of our current systematic strategy, we briefly described our published data here. Please refer to ref 9 for more experimental details. We recruited three healthy male blood donors and separated their plasma using all three separation techniques. Lipid-associated proteins were isolated, and their distributions across fractions were determined using high-performance liquid chromatography/electrospray ionization tandem MS (HPLC−ESI−MS/MS). GF separated each plasma sample into 17 successive size-based fractions across which 106 lipid-associated proteins were identified. The AE method separated plasma samples into 21 fractions and identified 140 lipid-associated proteins. IEF method identified 93 proteins in 20 fractions.

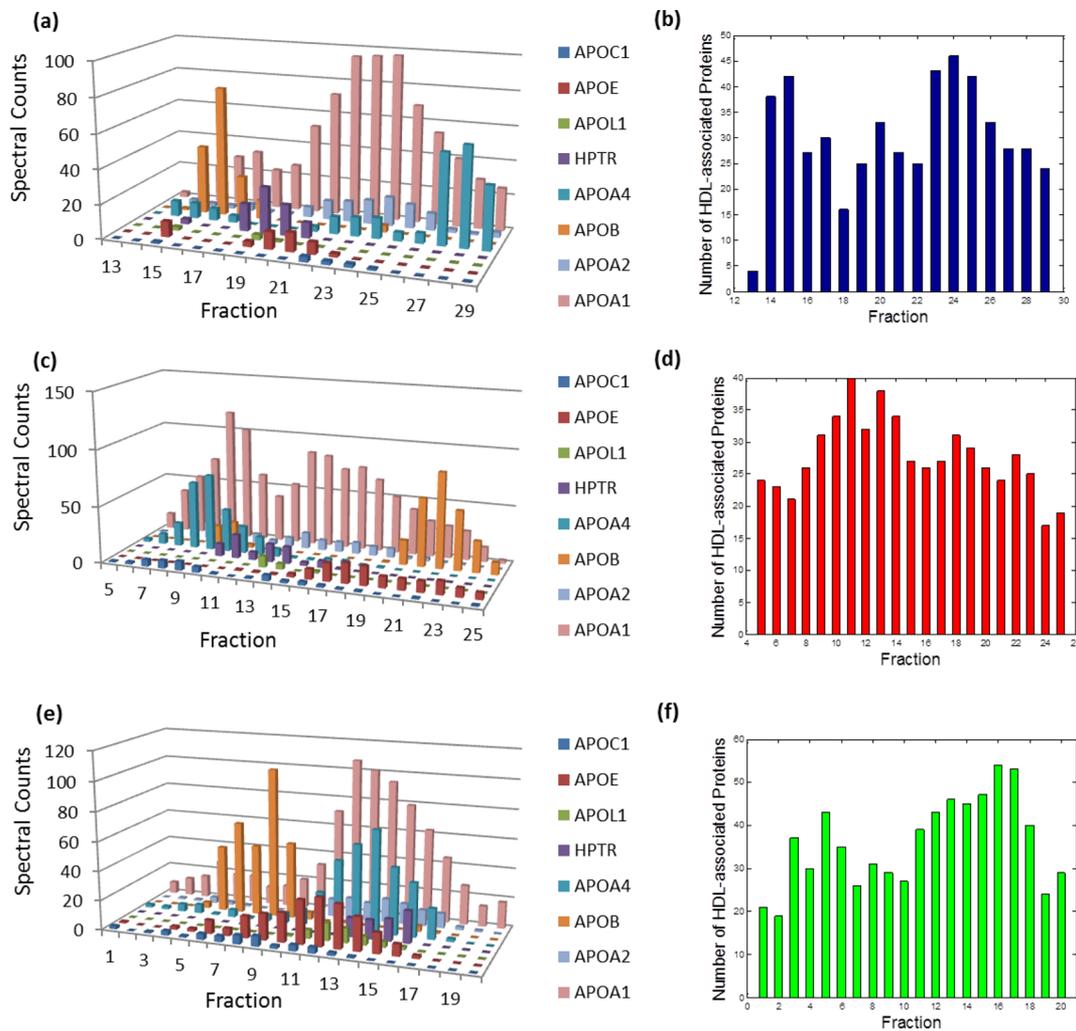### Human apoA-I Deficiency Disease Study

An apoA-I deficient female participant (age 40) was paired with a control female participant (age 43). Both subjects have no known CVD, body mass indexes (BMIs) in the normal range, and normal blood pressure. Venous blood was collected from participants after a 12-h fast by a trained phlebotomist using BD Vacutainer Plus Plastic Citrate Tubes containing buffered sodium citrate (0.105 M) as an anticoagulant. Cellular components were pelleted by centrifugation at ∼1590g for 15 min in a Horizon mini-E (Quest Diagnostics) at room temperature. Plasma was stored at 4 °C until applied to the GF separation technique, always within 16 h. Details of GF assays are the same as in our previous work.[8] Samples were never frozen. Written consent was obtained from participants in compliance with institutional regulations. Compositional analysis of lipoprotein fractions was assayed for these two subjects. HPLC−ESI−MS/MS was used to determine the distribution patterns for proteins across fractions.

HDL Watch List

A comprehensive HDL-associated proteins watch list is being continuously maintained and updated by the Davidson lab at http://homepages.uc.edu/~davidswm/HDLproteome.html. The most up-to-date list has tracked 89 "likely" HDL proteins of 224 proteins from 16 independent studies, where likely HDL proteins are defined as those that appeared in at least three studies from three independent laboratories.

Local Spearman's Rank Correlation Coefficient Score

Local Spearman's rank correlation coefficient Score (S-score) was based on the Spearman's rank correlation coefficient of the local migration patterns, which is more tolerant to errors in low spectral counts produced by low-abundance proteins. To reflect the local similarity, a sliding window w was utilized to restrict the abundance profiles within a certain range of fractions. Because of individual differences, we normalize the protein abundance profile by dividing the maximum of spectral counts of all fractions for any given protein in one plasma sample. Suppose we have a protein abundance profile $X = (X_1,...,X_i,...,X_n)$ where X_i is the normalized spectral count of protein P_x in the fraction i. For each fraction i, we only considered the normalized protein spectral counts within the sliding window of w fractions $[i − (1/2)(w − 1),...,i + (1/2)(w − 1)]$, averaged from all v plasma samples into one abundance

Figure 2. Abundance profile examples of multiple HDL-associated proteins and number of proteins detected by MS within each fraction from the separation method (a,b) GF, (c,d) AE, and (e,f) IEF.

vector. The total number of fractions is w, and the index j denotes the jth fraction in the local abundance vector. Then, for each protein pair (P_x, P_y) in the fraction i, the local S-score for a given separation method was calculated by

$$S_i(P_x, P_y) = \frac{\sum_{j=1}^{w}(x_j - \bar{x})(y_j - \bar{y})}{\sqrt{\sum_{j=1}^{w}(x_j - \bar{x})^2 \sum_{j=1}^{w}(y_j - \bar{y})^2}}$$

where x_j and y_j are abundance ranks, obtained from the normalized spectral counts X_j and Y_j of the protein pair (P_x, P_y) in the jth fraction for all plasma samples from one separation approach. Local S-score is a real number in the range of $[-1, 1]$. Local S-score is highly effective at measuring a monotonic similarity between variables by considering the rank of normalized abundance levels, and it also alleviates the bias against low-abundance proteins.

Functional Enrichment Analysis

We collected function annotations of human HDL-associated proteins from the GO Web site. For each of the identified subparticle candidates, to examine whether it is enriched within a certain function, we used the hypergeometric test to test the *null hypothesis* that proteins within one subparticle were picked randomly from the 89 master HDL proteins list. The p-values were calculated by

$$\sum_{i=q}^{p} \frac{\binom{p}{i}\binom{n-p}{m-i}}{\binom{n}{m}}$$

where n is the total number of genes on the watch list, m is the number of genes in the clique, p is the number of genes on our watch list associated with the given GO term, and q is the number of genes in this clique that were also associated with that GO term. The smaller the p-value is, the more significant the clique is enriched with the given function.

Lag-Score

We developed a lag-score (L-score), reflecting a quantitatively shifted distribution for a given protein. Although our local S-score is also able to detect the local dissimilarities between the migration patterns for any given fraction, our L-score is able to measure the global pattern differences in term of the shifted fractions across all the fractions. The L-score was calculated based on time-lag between the normalized aggregated abundance profiles for protein P_x from wild type (WT) and gene knockout (KO) mice groups. Time-lag is a concept in electronic signal processing to measure the shift between two signals. We applied this concept here to discover the migration patterns change between WT and KO groups. Assuming m WT

mice and n KO mice, L-score L^x of a given protein P_x between WT and KO groups was obtained by

$$L^x = \mathcal{F}\left(\frac{1}{\mu} \sum_{k=1}^{m} X_{wt}^k, \frac{1}{\nu} \sum_{l=1}^{n} X_{ko}^l \right)$$

where X_{wt}^k, X_{ko}^l are the normalized spectral counts vectors (i.e., abundance profiles) of protein P_x from kth WT mouse and lth KO mouse, respectively. Also, $\mu = \max(\Sigma_{k=1}^{m} X_{wt}^k)$, $\nu = \max(\Sigma_{l=1}^{n} X_{ko}^l)$. $\mathcal{F}$ is time-lag function to calculate signal lag in signal processing with cross-correlation. Cross-correlation is a similarity measure between two waveforms as one of them has time lag from the other. For discrete functions, the cross-correlation is an array defined as

$$(f * g)[i] \underset{\text{def}}{=} \sum_{m=-\infty}^{\infty} f*[m] g[m + i]$$

where $f*[m]$ denotes the complex conjugate of f, and m is the time-lag. Time-lag $\mathcal{F}(f, g)$ between two signals is the distance between the center and the maximum of the cross-correlation vector. Larger L-score indicates more significant fractions shifts of protein migration pattern due to the ablation of genes. L-score is an integer, either positive or negative, reflecting distribution shifts positively or negatively.

Spoke and Matrix PPIs Models

A spoke model assumes all impacted proteins in Tables 2 and 3 only interact with the absent protein (Figure S1a, Supporting Information). It is a direct interpretation of gene knockout experiments. In contrast, a matrix model assumes interactions among all proteins, including absent and pattern shifted proteins (Figure S1b, Supporting Information). We established three matrices to represent all interactions among all proteins (absent and pattern-shifted proteins). By using either model, PPIs derived from gene knockout experiments are able to serve as direct pieces of evidence that two interacting proteins may colocalize within the same subparticle. Thus, we directly utilized the number of edges (PPIs) being supported by the matrix and spoke models as the evidence in Table 1.

■ RESULTS

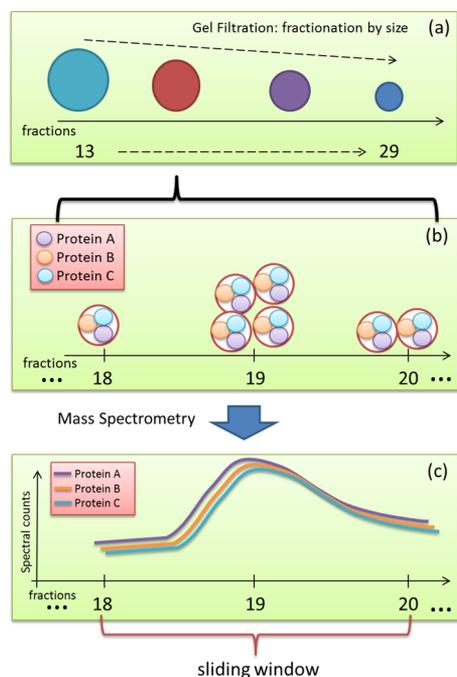### Fractionation of HDL Proteomics Data Set

Lipid associated proteins' distribution data set (see Material and Methods) was obtained in our previous study,[9] where healthy human plasma was fractionated by three optimized nondensity based orthogonal chromatographic separation techniques (GF, AE, and IEF). We first filtered an HDL-associated protein data set from original lipid associated protein data. Many research groups have used different proteomic techniques to study HDL compositions, and each approach assessing HDL fractionation reflected specific physicochemical properties of the particles such as density, size, and electrophoretic mobility. Because of the differences in HDL separation techniques, sample preparation, and instruments, the total list of HDL proteins varies dramatically from study to study. We have compared the existing data from 16 proteomics studies published to date and compiled a list of 89 high-confidence HDL-associated proteins that were observed in at least three different studies or have independent biochemical evidence of HDL residence (see Material and Methods). Therefore, we mainly focused on these 89 high-confidence HDL-associated proteins here and removed other data.

Abundance profiles of several known HDL-associated proteins from three separation techniques were presented (Figure 2a,c,e). As expected, the most abundant protein, apoA-I, occurred in nearly every fraction, while other apolipoproteins displayed relatively distinct distributions. Intriguingly, we noticed that only a portion of proteins co-occurred when we took a closer look at any individual fraction (Figure 2b,d,f). Additionally, many proteins, except the abundant ones, only existed in certain fractions rather than across the whole spectrum. The diversity of these proteins' distributions implicitly reflected the heterogeneity of HDL subspecies. HDL proteins coexisting within the same subparticles should travel together during the plasma separation; thus, proteins on a given subparticle are likely to be detected by MS in the same fraction. Hence, we first separated all proteins discovered in our experiments into different groups based on their coexistence in individual fractions. Consequently, the entire proteomics data pool was divided into 58 subsets based on GF (17 fractions), AE (21 fractions), and IEF (20 fractions) separation techniques. Although the total number of identified proteins in the three separation methods was 159, proteins coexisting within the individual fraction were commonly fewer than 40. It is possible that those coexisting proteins may come from more than one subspecies. However, the separation of detected proteins into subsets effectively distinguished "likely" and "unlikely" colocalized proteins. With the help of the following analyses, we were able to uncover the composition of certain subspecies.

Construction and Graph Analysis of Local Comigration Networks To Identify HDL Subspecies

Individual comigration networks were constructed for each fraction from the different separation techniques to represent the comigration relationship between any pair of HDL proteins. Vertices of the network for a given fraction represented MS-detected HDL-associated proteins. Edges between vertices represented the local comigration relationship, and each one is associated with a similarity score. Here, we developed a novel score, named local Spearman's rank correlation coefficient score (local S-score) (see Material and Methods) to quantitatively measure such local similarities (Figure 3). Conventionally, variables with a correlation coefficient larger than 0.8 are regarded as strongly correlated. As such, we chose the similarity threshold of 0.8 to transfer our weighted graphs to binary graphs. By using this multinetwork strategy, we constructed a total of 58 protein local comigration networks (17, 21, and 20 networks for GF, AE, and IEF techniques, respectively). Those 58 comigration networks have very diverse topologies, indicating the heterogeneity of subspecies' composition. To illustrate the overall structure of the HDL interactome, we merged the 58 comigration networks to form a comprehensive HDL interactome map that contains 70 proteins, 1540 edges (Figure S2, Supporting Information).

Within each comigration network, if all proteins included in one subspecies have similar migration patterns, they tend to form a highly connected cohesive network module. In graph theory, a clique in a network is a fully connected subset of the vertices where every two nodes in this subset are connected by an edge. A maximal clique is a clique that cannot be extended by including any more adjacent nodes, and it has been applied in protein networks to discover core network elements.[29] The maximal clique concept fits well with our purpose of discovering such highly connected cohesive modules. Figure 4

Figure 3. Rationale of local S-score for capturing the local similarity of proteins' migration patterns. (a) The mechanism of our separation methods utilizes different characteristics of each subspecies to create their specific distributions, that is, migration patterns. For example, in the GF approach, larger size subparticles are likely to migrate fast and fall into early fractions, while smaller size ones would be detected in the following fractions. (b) Successive neighboring fractions may contain the same type of particles. The same subparticles may distribute among multiple neighboring fractions in a specific pattern, for example, one subparticle containing proteins A, B, and C may distribute as shown in the figure. (c) Those proteins within the same subspecies are likely to have highly similar migration patterns locally. This local similarity may be only reflected within a certain range of fractions, that is, sliding window.

illustrates a local comigration network constructed for 19th fraction of GF method and one of maximal cliques within this network. In this study, we identified all maximal cliques using the Bron−Kerbosch algorithm[30] from individual comigration networks. Please note that we required a clique to contain at least three nodes as a protein complex and dismissed all two-node cliques that represent pairwise PPIs. Those discovered maximal cliques represented the likely protein complex candidates and were subject to further validation as follows.

The molecular weight was applied as a filter to remove any unlikely candidate. The molecular weight of an HDL complex is usually observed to be less than 400 000 Da, including roughly 50% (by mass) HDL-associated proteins and 50% (by mass) lipids.[31,32] Accordingly, we set a conservative upper limit of molecular weight for HDL subspecies as 200 000 Da. After all cliques were filtered with this molecular weight threshold, 183 candidates (Table S1, Supporting Information) were selected for further investigation. Because of the inability to directly observe a given subspecies, we had to look for multiple lines of indirect evidence to test identified subspecies candidates. We tested those subspecies with six lines of evidence, including: literature analysis, GO functional analysis, two PPIs models based on our mouse HDL study, and two PPIs models based on our human genetic deficiency disease study. Finally, we presented 38 putative HDL subspecies that are supported by at

least three lines of evidence (Table 1). In the following sections, we present independent lines of evidence that support the validity of the identified putative HDL subspecies.

Comparison of Our Local-Network Approach with Four Traditional Methods on Network Construction and Clique Identification

We first assessed the accuracy of the predicted HDL interactome network based on known HDL PPIs deposited in the Human Protein Reference Database (HPRD), where all PPIs were collected from published literature based on experiments (e.g., yeast-2-hybrid, co-IP, etc.) and manually curated to avoid errors.[33] The 352 PPIs involving 64 HDL proteins represent a comprehensive collection of known HDL PPIs, and we believed it is an ideal data set to test the coverage of our predictions in terms of pairwise interactions. All the reported PPIs related to HDL-associated proteins were used as positive instances, and all unreported ones were treated as negative instances.

On the basis of this gold-standard data set, we compared the performance of our local-network method to a simpler, more widely used method (i.e., constructing a single-network with a global similarity score derived based on distribution across all fractions) in terms of PPIs prediction. We tested the PPIs prediction on the traditional model and our models with various sliding windows w. Figure 5 shows receiver operating characteristic (ROC) curves, common graphical plots illustrating the performance of a binary classifier. For each predictive model, we calculated the area under the curve (AUC), which is equal to the probability that a given scoring system will return a higher score for a random positive PPI than the one for a random negative PPI. The higher the AUC, the better a predictive method. Our local-network models with ($w = 5$ or $w = 7$) had the highest AUC of 0.71, while the AUC of the model ($w = 3$) was 0.69. In contrast, the AUC of the traditional score was 0.65. The results indicate our local-network method has a better performance in predicting PPIs. Since the smaller sliding window requires less computational time, ($w = 5$) sliding window becomes the preferred parameter in the following analyses.

Alternatively, we conducted an analysis to construct three PPI networks from three separation methods (see Supporting Information, Figure S3a−c) and only considered the overlapping edges among all networks. The consensus network only consists of five well-known PPIs with negligible coverage (5/352) of known HDL PPIs (Figure S3d, Supporting Information). This comparison suggests that our local-network method was tolerant of a potential artifactual lack of comigration due to experimental perturbation in one of the separations; thus, the failure of a given complex to survive one of the separations does not necessarily preclude the identification of the subspecies. Each of the separation methods has drawbacks that can potentially perturb particle migration or integrity, for example, dilution effects in GF and salt effects in AE. The conventional method that only considers the simultaneously coassociated protein pairs among all three separation methods may yield a very limited number of PPIs.

In the third comparison, we found many PPIs that can only be discovered by our method but not a traditional method. In our previous study,[9] we have applied a traditional global correlation analysis across all fractions to identify a few highly correlated protein pairs, for example, fibrinogen alpha chain (FGA):fibrinogen beta chain (FGB), FGB:fibrinogen gamma

Figure 4. A local comigration network constructed for 19th fraction of GF method. Size of the vertex reflects network degree of this vertex. Circled subnet is a maximal clique within this network, corresponding to the well-known TLF particle.

chain (FGG), and apoA-I:apoA-II.[9] The top ranked pairs discovered in our previous study were confirmed once again in this work. In addition to those pairs, our new score is able to reveal more comigrated relations that could not be reflected in conventional correlation analysis. For example, apoA-I: apoL-I, an interaction observed in other independent studies,[21,22] and in our human apoA-I deficiency study, was discovered by our local comigration analyses in several fractions. However, the migration patterns of apoA-I and apoL-I were not strongly correlated across all fractions, and therefore the interaction was not identified in our previous study.

Finally, we explored whether distinct HDL complexes could be uncovered from the densely connected merged HDL interactome (Figure S2, Supporting Information) rather than from 58 individual local networks. We noted that the complexes identified by the graph mining algorithms in such a densely connected network often have molecular weights that are too large for HDL particles. This may be due to that HDL proteins, especially the abundant ones, are likely to participate in different subparticles and interact with distinct proteins[8,9,34] so that the traditional single-network strategy is likely to uncover a large protein complex that involves multiple subparticles in reality. Apparently, such diverse characteristics of HDL complexes cannot be properly represented with static links in one conglomerate protein interactome map.[35]

Each of the Putative HDL Subspecies Has at Least Two Literature Supports

We first examined the PPIs within identified HDL complexes using the reported PPIs in HPRD database. The complexes with more reported PPIs are likely to exist in reality. Each of 38 HDL subspecies has multiple literature supports. With the HPRD database and literature review, we presented the number of PPIs supported by literature for each individual HDL subspecies in Table 1.

The most recognized HDL subparticle, the TLF particle (apoA-I, apoL-I, and HPR) was discovered from several fractions in our analysis, demonstrating the effectiveness of our systematic strategy. The network in Figure 4 is one of the comigration networks containing this TLF particle. Our local S-score between apoL-I and HPR was up to 0.97 (*p*-value = 0.017). In contrast, we performed coexpression-based PPI prediction on STRING[36] by querying either apoL-I or HPR, and PPI between apoL-I and HPR was not presented. Also, the traditional global score between apoL-I and HPR reported in our previous work is only up to 0.72 among three separation methods, below the required correlation threshold of 0.8.

We also looked for other independent studies to support the existence of our subparticle candidates. One example is the apoA-I, apoC-I, and apoE complex.[37,38] It has been reported that apoC-I binds free fatty acids and reduces their intracellular esterification, and its function to modulate the interaction of apoE and beta-migrating VLDL.[39] At the same time, apoE and apoA-I binding to ATP-binding cassette, subfamily A member 1 (ABCA1) is essential for the HDL formation.[40] ApoA-I mainly works in the cholesterol efflux process, and many studies have supported the idea that apoC-I and apoE may work together with apoA-I to help with lipid metabolism. We may infer from this prior knowledge that the complex (apoA-I, apoC-I, and apoE) may exist in certain molecular processes.

Another example is complex (apoA-I, apoA-II, Complement factor B, and Transthyretin), whose all pairwise PPIs were supported by literature. Transthyretin (TTR), the plasma carrier for both thyroxine and retinol, has connections to apoA-I.[41,42] TTR was shown to affect HDL biology and the development of atherosclerosis by reducing cholesterol efflux and increasing the apoA-I amyloidogenic potential.[43] It was shown that TTR can cleave apoA-I, decreasing its ability to promote cholesterol efflux from cholesterol-loaded macro-

Table 1. Putative HDL Subspecies That Are Supported by at Least Three Lines of Evidence

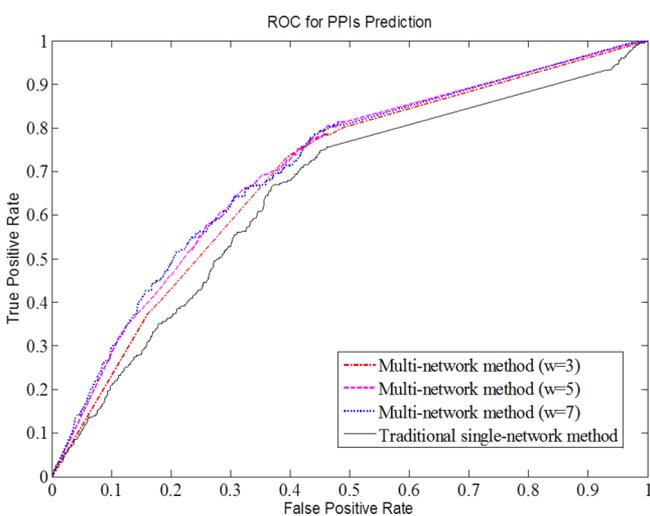| size	subspecies					literature	GO enrichment	mouse matrix	mouse spoke	human matrix	human spoke
3	APOA1	CLU	HPR			2	3.92×10^{-03}	1	1	3	2
3	APOA1	APOL1	CLU			2	3.92×10^{-03}	1	1	3	2
3	APOA1	APOL1	HPR			2	5.87×10^{-02}	0	0	3	2
3	APOA1	APOE	SERPING1			3	6.17×10^{-03}	3	2	0	0
3	APOA1	APOE	ITIH1			3	6.17×10^{-03}	3	2	0	0
3	APOA1	APOC3	PON1			2	6.17×10^{-03}	3	2	3	2
3	APOA1	CLU	SERPIND1			2	3.92×10^{-03}	3	2	1	1
3	APOA1	APOC2	GPLD1			2	1.38×10^{-02}	3	1	3	2
3	APOA1	APOA2	APOC1			3	2.49×10^{-03}	3	3	3	2
3	APOA1	APOC3	APOE			3	4.05×10^{-04}	3	2	1	1
3	APOA1	APOA2	ITIH1			3	3.92×10^{-03}	3	3	1	1
3	APOA1	APOC3	CLU			3	3.92×10^{-03}	3	2	3	2
3	APOA1	APOA2	APOC3			3	4.05×10^{-04}	3	3	3	2
3	APOA1	APOC1	CLU			3	3.92×10^{-03}	3	2	3	2
3	APOA1	APOC2	APOC3			3	1.62×10^{-03}	3	1	3	2
3	APOA1	APOC1	APOE			3	2.49×10^{-03}	3	2	1	1
3	APOA1	APOC2	PON1			2	1.38×10^{-02}	3	1	3	2
3	APOA1	APOA2	APOA4			3	4.05×10^{-04}	2	2	1	1
4	ALB	APOA1	APOE	SERPING1		6	8.95×10^{-03}	3	2	0	0
4	APOA1	APOC1	APOC3	HP		6	5.92×10^{-03}	4	2	3	2
4	APOA1	AHSG	HPX	SERPIND1		4	8.84×10^{-02}	3	2	1	1
4	ALB	APOA1	APOC1	CFB		6	1.56×10^{-02}	3	2	1	1
4	ALB	APOA1	APOA2	APOC1		6	3.92×10^{-03}	3	3	3	2
4	ALB	APOA1	APOC1	HPR		4	1.56×10^{-02}	1	1	3	2
4	APOA1	APOA2	CLU	F2		4	6.00×10^{-03}	3	3	3	2
4	APOA1	APOC1	APOE	GSN		6	3.92×10^{-03}	3	2	1	1
4	APOA1	APOA2	CFB	TTR		6	6.00×10^{-03}	2	2	1	1
5	APOA1	APOA2	APOC3	SERPING1	IGHG1	10	1.62×10^{-03}	5	4	3	2
5	APOA1	APOA2	APOA4	IGHG1	PON1	7	1.62×10^{-03}	4	4	3	2
5	APOA1	APOA2	APOE	IGHG1	F2	10	3.92×10^{-03}	3	3	1	1
5	APOA1	APOA2	APOC3	F2	TTR	10	1.62×10^{-03}	3	3	3	2
5	APOA1	APOA2	CLU	F2	TTR	8	6.35×10^{-03}	3	3	3	2
5	APOA2	APOC3	APOM	F2	TTR	6	6.35×10^{-03}	3	2	3	0
5	APOA2	APOM	CLU	F2	TTR	4	1.38×10^{-02}	3	2	3	0
5	APOA1	AHSG	HP	SERPING1	TTR	10	8.01×10^{-02}	3	2	1	1
5	APOA1	APOA2	APOA4	HPX	SERPIND1	7	1.62×10^{-03}	3	3	1	1
5	APOA1	APOA2	CFB	HP	TTR	10	6.35×10^{-03}	3	2	1	1
5	APOA1	APOC3	CFB	CLU	TTR	9	6.35×10^{-03}	6	3	3	2

Figure 5. ROC curves for the traditional score and our local S-score with various sliding windows *w*.
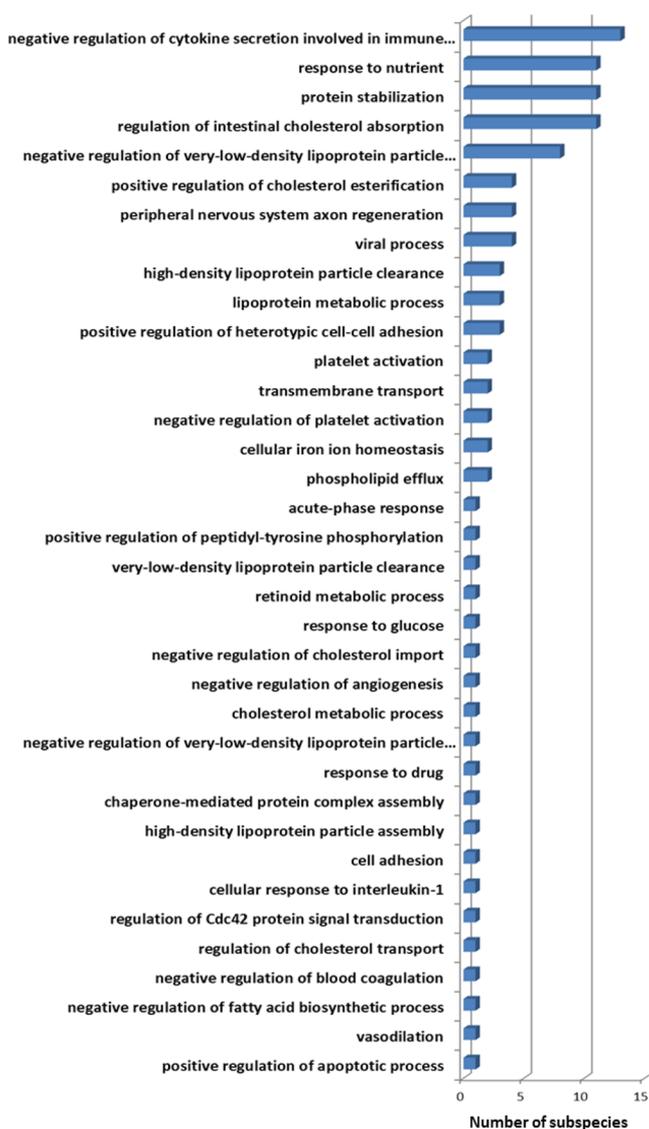
phages.[44] Moreover, the apoA-I cleaved by TTR has reduced affinity for ABCA1, as assessed by cross-linking.[45] These support the notion that this particle may exist and play a critical role in cholesterol efflux.

Diverse Biological Functions of HDL Complexes

Being enriched for biological functions supports the existence of the protein complex candidates. For each of the identified subspecies, to examine whether it is enriched for certain GO terms, the hypergeometric test was used to test the significance against the null hypothesis, that is, all proteins clustered as one subparticle were picked randomly from the HDL watch list (see Material and Methods). In Table 1, we only listed the *p*-value corresponding to the most significant GO terms. Of the 38 subspecies candidates, 31 have significantly enriched functions after Benjamini correction (*p*-value < 0.01). Take the case of subparticle (apoA-I, apoA-II, and apoA-IV), for example, with the most significant annotation of "regulation of intestinal cholesterol absorption" (*p*-value: 5.37×10^{-04}). Its individual members commonly participate in the cholesterol metabolism

process,[46−48] suggesting that this subparticle may exist in nature and perform a specific metabolic function.

To examine the variety of GO terms enriched among the 183 subparticle candidates, we summarized the frequency of the most significant GO terms associated with individual putative subspecies in Figure 6. Several enriched GO terms of identified

Figure 6. Histogram of the most significantly enriched functions of 38 identified HDL subspecies. Distribution of the functions covers both fundamental biological functions and CVD-protective functions.

subparticles turn out to be the annotation of fundamental biological processes. Those functions are essential to keep the normal cellular activity, for example, "positive regulation of heterotypic cell–cell adhesion". On the other hand, several other enriched functions are consistent with previously known HDL functions such as "reverse cholesterol transport", "antioxidation", "immune response", and "hemostasis". Although the CVD protective functions have been the major focus of various HDL studies, our results suggested that distinct HDL subspecies may be responsible for different function-alities, from fundamental biological functions to CVD-protective functions. We are aware that the current GO knowledge may be incomplete; however, since it was not our

intention to discover new HDL biological functions based on the current GO knowledge, the GO enrichment analysis primarily served the purpose to validate reasonable protein clustering in that irrelevant proteins in term of GO functions should not dominate the candidate subparticles.

Validation of HDL Subspecies Using a Mouse HDL Study

To study the composition of HDL subspecies, we have utilized a data set from our mouse HDL study[49] and analyzed protein distribution patterns of mice when three major HDL-associated genes (*APOA1*, *APOA2*, and *APOA4*) were knocked out individually. The mouse model is an invaluable system for the study of genetic effects on lipoprotein metabolism. Their plasma contains lipoproteins that are roughly similar to those in the human in terms of protein and lipid composition.[50] Plasma separation and MS analysis assays were performed for three WT mice and three KO mice in three genetic knockout experiments, respectively. Please refer to ref 49 for more experimental details on our mouse HDL study. Here, we hypothesized that two proteins are likely to coexist on the same protein complex if one of them has a shifted distribution after another is absent (Figure S4a, Supporting Information). On the other hand, two proteins are less likely to coexist on the same particle if one protein has no distribution change after another is ablated (Figure S4b, Supporting Information). To quantitatively evaluate the shifting of the proteins' distribution patterns, we developed a lag-score (L-score) migration pattern shift analysis (see Material and Methods). Proteins with $|L| \geq 1$ were identified as influenced proteins. Then, the identified mouse proteins were mapped back to human HDL-associated proteins by sequence homology.

With our L-score, we inferred 26, 16, and 4 human HDL-associated proteins from the mouse HDL study with the ablation of *APOA1*, *APOA2*, and *APOA4*, respectively. All influenced proteins and their corresponding L-scores are listed in Table 2. The absolute value of L-score indicates the significance level of pattern changes. Small absolute value indicates that only subtle changes were detected, while large absolute value indicates obvious change of the migration patterns. Proteins were ranked with the absolute value of L-score. The ablation of *APOA1* had a significant impact on the distribution of 26 other HDL-associated proteins. The ablation of *APOA2* had a smaller effect on 16 mapped HDL-associated proteins. Only apoA-II, apoC-III, HPR, and Haptoglobin (HP) were identified during the protein mapping according to the *APOA4* knockout experiment. Both spoke and matrix PPIs models[27] were adopted to determine the validity of the identified subspecies (see Material and Methods). Among 38 putative complexes, 37 subparticles are supported by at least one PPI with the spoke PPIs model, while 37 subspecies have at least one PPI supported by the matrix PPIs model (Table 1).

Validation of the Identified Subspecies with Human apoA-I Deficiency Disease Study

To provide further information in the human system, we obtained a plasma sample from a patient with familial apoA-I deficiency. The genetic deficiency of apoA-I is extremely rare and has been reported in only 16 families throughout the world.[51] Because of the rarity of this type of mutation in humans, larger-scale studies on this population would be extremely difficult, and we were able to recruit only one participant for this study. It is also interesting to note that although these patients have markedly reduced plasma HDL-C levels, usually around 20−25 mg/dL, there is no clear

Table 2. Human HDL-Associated Proteins Identified in the Migration Pattern Shifting Analysis. Each Column Lists All the Influenced Proteins, Ranked by Absolute Value of Their L-Scores, Due to the Absence of One Apolipoprotein in the Mouse Model

apoA-I		apoA-II		apoA-IV	
influenced proteins	L-score	influenced proteins	L-score	influenced proteins	L-score
SAA4	10	APOC1	12	APOA2	1
AZGP1	9	APOC2	11	HP	1
PON1	6	APOC3	2	HPR	1
GPLD1	2	GPLD1	2	APOC3	−1
APOC3	−2	APOA1	1		
AHSG	−1	APOE	1		
AMBP	−1	APOM	1		
APOC1	−1	AZGP1	1		
APOE	−1	ITIH2	1		
CLU	−1	ITIH1	1		
C1S	−1	ITIH4	1		
C9	−1	AMBP	1		
CFB	−1	PON1	1		
C2	−1	CLU	−1		
ITIH2	−1	C9	−1		
ITIH1	−1	CFH	−1		
LUM	−1				
PGLYRP2	−1				
SERPINA1	−1				
SERPINA3	−1				
SERPING1	−1				
SERPINA4	−1				
SERPINF1	−1				
SERPINC1	−1				
SERPIND1	−1				
SERPINF2	−1				

Table 3. Human apoA-I Deficiency Influenced HDL-Associated Proteins. Proteins Were Ranked by the Absolute Values of Their L-Scores

influenced proteins	L-score
APOL1	10
GPLD1	10
APOC1	8
APOC2	8
SAA4	8
HPR	6
APOM	4
APOC3	3
PON1	−3
APOA2	−1
APOH	−1
CLU	−1
AHSG	−1
ITIH4	1
KLKB1	−1
RBP4	−1

least one PPI directly supported by the spoke model. With the matrix model, 35 subspecies had at least one PPI being supported.

■ DISCUSSION

In this study, we systematically identified and characterized structural HDL subspecies through analysis of proteins' comigration patterns generated by three orthogonal chromatographic separation techniques. Current studies of HDL proteomics are few and are limited in that, by only looking at pools of total HDL or very broad density subsets (i.e., HDL2 or HDL3), they do not take into account the heterogeneity of the HDL population. In contrast, our proteomic experiments fractionated the total HDL pool more extensively to enable discrimination between distinct subspecies. Greater fractionation of the total HDL population allows us to examine protein variances between particles more closely and identify specific HDL subspecies. To take full advantage of our separation techniques, a multinetwork-based approach was employed to study subspecies composition. This work is novel in the following respects.

First, most existing studies on HDL complexes, including our previous work, are limited by focusing on pairwise HDL PPIs. In contrast, our research aimed at systematically inferring HDL subspecies by identifying protein complexes. A major difficulty in the current attempts to study HDL subspecies is the lack of a direct experimental approach to reveal and validate the protein composition in individual subspecies. As such, we proposed an integrative approach by combining experimental fractionation, computational inference, and multidimensional validation. In this paper, we presented 38 candidate protein complexes, which have not been published before.

Second, to achieve our goal of identifying protein complexes in HDL subspecies, we reanalyzed our previously published proteomics data by deploying novel computational approaches. For example, we developed a novel local S-score, which maximally captures the migration similarities between proteins' abundance profiles, and a multinetwork strategy to construct 58 local comigration networks for individual fractions, rather than one conglomerate protein network, for increasing the resolution for subspecies discovery. These novel approaches

association with an increased occurrence of CVDs.[34] Similar to the rationale of the mouse model study, the deficient proteins are likely to disrupt the formation or at least change the molecular size of the corresponding subspecies. Details of assays are described in the Material and Methods. Forty-one known HDL-associated proteins were identified among a total of 103 MS-detected proteins.

Migration pattern shift analysis was performed similar to that conducted in the mouse study. Of the 41 MS-detected HDL-associated proteins, 16 were determined to have a shift in distribution patterns with L-score ($|L^x| \geq 1$) (Table 3). Proteins were ranked with the absolute value of L-score. Some migration pattern comparison examples are shown in Figure S5 of the Supporting Information. ApoA-I migration patterns were first provided to show the lack of apoA-I in the patient compared to the healthy control. Another major protein, apoA-II, was detected with minor shift in our analysis (L-score = −1). Next, we found that both HPR and apoL-I cannot be detected in the lipoprotein fractions of the patient plasma, which is consistent with the TLF particle reported by Rifkin and Raper et al.[21,22] Additionally, apoC-I and apoC-II's migration patterns were shifted similarly (L-score = 8), suggesting that they may coexist with apoA-I on certain complexes. Indeed, subparticle (apoA-I, apoC-I, and apoC-II) was discovered in our analysis (Table 1).

Again, both matrix and spoke PPIs models were adopted for this apoA-I deficiency study to test the identified subspecies. Thirty-three of the 37 subparticles containing apoA-I had at

enable us to infer distinguishable HDL subspecies in the analyses.

Finally, multidimensional substantial experiments as well as computational analysis were performed to test the validity of the identified subspecies in this study. Gene knockout data sets from *APOA1*, *APOA2*, and *APOA4* deficient mice were utilized. Analyses results have not been published, although the experimental details were discussed in our previous work. Furthermore, a novel human genetic deficiency study was applied for our complex validation. In this study, one apoA-I deficient patient was studied to look at the associated complexes. Additionally, literature searching and GO functional enrichment were used to test our putative complexes. The putative HDL complexes with multiple pieces of evidence from the validations are the highly confident candidates for future biochemical studies aimed at determining HDL protein physical interactions or colocalization, for example, immunoprecipitation.

Because of the limitation of discover-type MS proteomics experiment, some low-abundance HDL-associated proteins were not found in our MS scanning, such as phospholipid transfer protein (PLTP). A targeted MS/MS scanning may improve data acquisition quality. In spite of the missing peptides in the MS scanning, it is fortunate that our analysis pipeline is independent of the completeness of MS data. Our identified putative HDL complexes in Table 1 would not be compromised since they may only represent subsets (sub-particles) of HDL particles in nature.

Our future work will focus on associating the putative subspecies to their biological functions. Particularly, we are more interested in those low-abundance proteins that are newly identified. One idea is that apoA-I and apoA-II act as organizing scaffolds for proteins that principally mediate the classical lipid transport roles of HDL.[52,53] However, lower-abundance proteins, many of which have putative functions that differ quite significantly from lipid transport, may represent the most promising candidates for participation in distinct HDL subspecies. Indeed, this has been demonstrated in the case of the TLF particle, which contains HPR and apoL-I.[21,22] This particle clearly plays a major role in innate immune function with an abundance level too low to play a meaningful role in lipid transport. Further studies will be needed to determine if some of the putative subspecies identified here have similar distinctive functions.

Overall, our work is the first report that employs MS-determined local comigration patterns and graph pattern mining to systematically infer HDL subspecies with individual high-resolution networks. It uncovered the composition of some HDL subspecies with a novel multinetwork computational approach. Our work also has significant implications in current cardiovascular disease research. A better understanding of the HDL subspecies that are either protective against or permissive to CVD will lead directly to new diagnostic tests for these species. For example, if we find that a particular subspecies is correlated with the development of CVD, we can envision screening CVD patients for this deleterious HDL subspecies in a clinical assay. Furthermore, existing therapeutics tend to boost HDL-C levels indiscriminately without regard for functions; and since HDL comprises numerous particle populations, simply raising HDL-C may increase the wrong sorts of particles at the expense of the cardio-protective ones. Therefore, identification of CVD-protective HDL subspecies

may help focus on new HDL-raising therapies that offer more specificity than those currently under exploration.

ASSOCIATED CONTENT

S Supporting Information

Supporting figures for alternative layouts of HDL interactome map combining all individual local networks. HDL interactome maps for GF, AE, and IEF methods based on global correlation scores and HDL interactome map containing coassociated PPIs among three separation methods, migration pattern shifting analysis for mouse gene knockout experiments, protein migration pattern comparison between the apoA-I deficient patient and the normal control, and spoke and matrix model for protein−protein interactions. Description on a global score-based method. Supporting tables for full list of identified HDL subspecies. The Supporting Information is available free of charge on the ACS Publications website at DOI: 10.1021/acs.jproteome.5b00419.

AUTHOR INFORMATION

Corresponding Author

*E-mail: Long.Lu@cchmc.org. Phone: 513-636-8720. Fax: 513-636-2056.

Notes

The authors declare no competing financial interest.

ACKNOWLEDGMENTS

ABBREVIATIONS

HDL, high-density lipoprotein; apo, apolipoprotein; CVD, cardiovascular disease; CETP, cholesteryl ester transfer protein; PLTP, phospholipid transfer protein; RCT, reverse cholesterol transport; TLF, trypanosome lytic factor; UC, ultracentrifugation; GF, gel filtration; AE, anion exchange; IEF, isoelectric focusing; GO, Gene Ontology; S-score, Spearman's rank correlation coefficient score; L-score, lag-score; WT, wild-type; KO, knock out

REFERENCES

(1) Mahmood, S. S.; Levy, D.; Vasan, R. S.; Wang, T. J. The Framingham Heart Study and the epidemiology of cardiovascular disease: A historical perspective. *Lancet* **2014**, *383* (9921), 999−1008.

(2) Alwan, A. *Global Status Report on Noncommunicable Diseases 2010*; World Health Organization: Geneva, Switzerland, 2011.

(3) Rezaee, F.; Casetta, B.; Levels, J. H.; Speijer, D.; Meijers, J. C. Proteomic analysis of high-density lipoprotein. *Proteomics* **2006**, *6* (2), 721−30.

(4) Vaisar, T.; Pennathur, S.; Green, P. S.; Gharib, S. A.; Hoofnagle, A. N.; Cheung, M. C.; Byun, J.; Vuletic, S.; Kassim, S.; Singh, P.; Chea, H.; Knopp, R. H.; Brunzell, J.; Geary, R.; Chait, A.; Zhao, X. Q.; Elkon, K.; Marcovina, S.; Ridker, P.; Oram, J. F.; Heinecke, J. W. Shotgun proteomics implicates protease inhibition and complement activation in the antiinflammatory properties of HDL. *J. Clin. Invest.* **2007**, *117* (3), 746−56.

(5) Karlsson, H.; Leanderson, P.; Tagesson, C.; Lindahl, M. Lipoproteomics II: Mapping of proteins in high-density lipoprotein using two-dimensional gel electrophoresis and mass spectrometry. *Proteomics* **2005**, *5* (5), 1431−45.

(6) Heller, M.; Stalder, D.; Schlappritzi, E.; Hayn, G.; Matter, U.; Haeberli, A. Mass spectrometry-based analytical tools for the molecular protein characterization of human plasma lipoproteins. *Proteomics* **2005**, *5* (10), 2619–30.

(7) Davidson, W. S.; Silva, R. A.; Chantepie, S.; Lagor, W. R.; Chapman, M. J.; Kontush, A. Proteomic analysis of defined HDL subpopulations reveals particle-specific protein clusters: Relevance to antioxidative function. *Arterioscler., Thromb., Vasc. Biol.* **2009**, *29* (6), 870–6.

(8) Gordon, S. M.; Deng, J.; Lu, L. J.; Davidson, W. S. Proteomic characterization of human plasma high density lipoprotein fractionated by gel filtration chromatography. *J. Proteome Res.* **2010**, *9* (10), 5239–49.

(9) Gordon, S. M.; Deng, J.; Tomann, A. B.; Shah, A. S.; Lu, L. J.; Davidson, W. S. Multidimensional coseparation analysis reveals protein–protein interactions defining plasma lipoprotein subspecies. *Mol. Cell Proteomics* **2013**, *12* (11), 3123–34.

(10) Riwanto, M.; Rohrer, L.; Roschitzki, B.; Besler, C.; Mocharla, P.; Mueller, M.; Perisa, D.; Heinrich, K.; Altwegg, L.; von Eckardstein, A.; Luscher, T. F.; Landmesser, U. Altered activation of endothelial anti- and proapoptotic pathways by high-density lipoprotein from patients with coronary artery disease: Role of high-density lipoprotein-proteome remodeling. *Circulation* **2013**, *127* (8), 891–904.

(11) Sreckovic, I.; Birner-Gruenberger, R.; Obrist, B.; Stojakovic, T.; Scharnagl, H.; Holzer, M.; Scholler, M.; Philipose, S.; Marsche, G.; Lang, U.; Desoye, G.; Wadsack, C. Distinct composition of human fetal HDL attenuates its antioxidative capacity. *Biochim. Biophys. Acta* **2013**, *1831* (4), 737–46.

(12) Link, J. J.; Rohatgi, A.; de Lemos, J. A. HDL cholesterol: Physiology, pathophysiology, and management. *Curr. Probl. Cardiol.* **2007**, *32* (5), 268–314.

(13) Shah, A. S.; Tan, L.; Long, J. L.; Davidson, W. S. Proteomic diversity of high-density lipoproteins: Our emerging understanding of its importance in lipid transport and beyond. *J. Lipid Res.* **2013**, *54* (10), 2575–85.

(14) Glomset, J. A. The plasma lecithins:cholesterol acyltransferase reaction. *J. Lipid Res.* **1968**, *9* (2), 155–67.

(15) Mackness, M. I.; Arrol, S.; Durrington, P. N. Paraoxonase prevents accumulation of lipoperoxides in low-density lipoprotein. *FEBS Lett.* **1991**, *286* (1–2), 152–4.

(16) Nofer, J. R.; Assmann, G. Atheroprotective effects of high-density lipoprotein-associated lysosphingolipids. *Trends Cardiovasc. Med.* **2005**, *15* (7), 265–71.

(17) Wadham, C.; Albanese, N.; Roberts, J.; Wang, L.; Bagley, C. J.; Gamble, J. R.; Rye, K. A.; Barter, P. J.; Vadas, M. A.; Xia, P. High-density lipoproteins neutralize C-reactive protein proinflammatory activity. *Circulation* **2004**, *109* (17), 2116–22.

(18) Kulkarni, S.; Woollard, K. J.; Thomas, S.; Oxley, D.; Jackson, S. P. Conversion of platelets from a proaggregatory to a proinflammatory adhesive phenotype: Role of PAF in spatially regulating neutrophil adhesion and spreading. *Blood* **2007**, *110* (6), 1879–86.

(19) Kuvin, J. T.; Harati, N. A.; Pandian, N. G.; Bojar, R. M.; Khabbaz, K. R. Postoperative cardiac tamponade in the modern surgical era. *Ann. Thorac. Surg.* **2002**, *74* (4), 1148–53.

(20) Asztalos, B. F.; Schaefer, E. J. High-density lipoprotein subpopulations in pathologic conditions. *Am. J. Cardiol.* **2003**, *91* (7A), 12E–7E.

(21) Rifkin, M. R. Identification of the trypanocidal factor in normal human serum: High-density lipoprotein. *Proc. Natl. Acad. Sci. U. S. A.* **1978**, *75* (7), 3450–4.

(22) Raper, J.; Fung, R.; Ghiso, J.; Nussenzweig, V.; Tomlinson, S. Characterization of a novel trypanosome lytic factor from human serum. *Infect. Immun.* **1999**, *67* (4), 1910–6.

(23) Sawle, A.; Higgins, M. K.; Olivant, M. P.; Higgins, J. A. A rapid single-step centrifugation method for determination of HDL, LDL, and VLDL cholesterol, and TG, and identification of predominant LDL subclass. *J. Lipid Res.* **2002**, *43* (2), 335–43.

(24) van't Hooft, F.; Havel, R. J. Metabolism of apolipoprotein E in plasma high density lipoproteins from normal and cholesterol-fed rats. *J. Biol. Chem.* **1982**, *257* (18), 10996–1001.

(25) Havugimana, P. C.; Hart, G. T.; Nepusz, T.; Yang, H.; Turinsky, A. L.; Li, Z.; Wang, P. I.; Boutz, D. R.; Fong, V.; Phanse, S.; Babu, M.; Craig, S. A.; Hu, P.; Wan, C.; Vlasblom, J.; Dar, V. U.; Bezginov, A.; Clark, G. W.; Wu, G. C.; Wodak, S. J.; Tillier, E. R.; Paccanaro, A.; Marcotte, E. M.; Emili, A. A census of human soluble protein complexes. *Cell* **2012**, *150* (5), 1068–81.

(26) Spirin, V.; Mirny, L. A. Protein complexes and functional modules in molecular networks. *Proc. Natl. Acad. Sci. U. S. A.* **2003**, *100* (21), 12123–8.

(27) Bader, G. D.; Hogue, C. W. An automated method for finding molecular complexes in large protein interaction networks. *BMC Bioinf.* **2003**, *4* (1), 2.

(28) Lu, L. J.; Xia, Y.; Paccanaro, A.; Yu, H.; Gerstein, M. Assessing the limits of genomic data integration for predicting protein networks. *Genome Res.* **2005**, *15* (7), 945–953.

(29) Lin, C. C.; Juan, H. F.; Hsiang, J. T.; Hwang, Y. C.; Mori, H.; Huang, H. C. Essential core of protein–protein interaction network in *Escherichia coli*. *J. Proteome Res.* **2009**, *8* (4), 1925–31.

(30) Bron, C.; Kerbosch, J. Finding all cliques of an undirected graph [H]. *Commun. ACM* **1973**, *16* (9), 575–7.

(31) Gordon, S. M.; Hofmann, S.; Askew, D. S.; Davidson, W. S. High-density lipoprotein: It's not just about lipid transport anymore. *Trends Endocrinol. Metab.* **2011**, *22* (1), 9–15.

(32) Eisenberg, S. High density lipoprotein metabolism. *J. Lipid Res.* **1984**, *25* (10), 1017–58.

(33) Prasad, T. K.; Goel, R.; Kandasamy, K.; Keerthikumar, S.; Kumar, S.; Mathivanan, S.; Telikicherla, D.; Raju, R.; Shafreen, B.; Venugopal, A. Human protein reference database—2009 update. *Nucleic Acids Res.* **2009**, *37* (Suppl.1), D767–72.

(34) Santos, R. D.; Schaefer, E. J.; Asztalos, B. F.; Polisecki, E.; Wang, J.; Hegele, R. A.; Martinez, L. R.; Miname, M. H.; Rochitte, C. E.; Da Luz, P. L.; Maranhao, R. C. Characterization of high density lipoprotein particles in familial apolipoprotein A-I deficiency. *J. Lipid Res.* **2008**, *49* (2), 349–57.

(35) Zhang, M.; Lu, L. J. Investigating the validity of current network analysis on static conglomerate networks by protein network stratification. *BMC Bioinf.* **2010**, *11*, 466.

(36) Franceschini, A.; Szklarczyk, D.; Frankild, S.; Kuhn, M.; Simonovic, M.; Roth, A.; Lin, J.; Minguez, P.; Bork, P.; von Mering, C. STRING v9. 1: Protein–protein interaction networks, with increased coverage and integration. *Nucleic Acids Res.* **2013**, *41* (D1), D808–15.

(37) Schamaun, O.; Olaisen, B.; Mevag, B.; Gedde-Dahl, T., Jr.; Ehnholm, C.; Teisberg, P. The two apolipoprotein loci apo A-I and apo A-IV are closely linked in man. *Hum. Genet.* **1984**, *68* (2), 181–4.

(38) Ordovas, J. M.; Schaefer, E. J. Genetic determinants of plasma lipid response to dietary intervention: The role of the APOA1/C3/A4 gene cluster and the APOE gene. *Br. J. Nutr.* **2000**, *83* (Suppl. 1), S127–36.

(39) Puppione, D. L. Higher primates, but not New World monkeys, have a duplicate set of enhancers flanking their apoC-I genes. *Comp. Biochem. Physiol., Part D: Genomics Proteomics* **2014**, *11*, 45–8.

(40) Karten, B.; Campenot, R. B.; Vance, D. E.; Vance, J. E. Expression of ABCG1, but not ABCA1, correlates with cholesterol release by cerebellar astroglia. *J. Biol. Chem.* **2006**, *281* (7), 4049–57.

(41) Monaco, H. L. The transthyretin-retinol-binding protein complex. *Biochim. Biophys. Acta* **2000**, *1482* (1–2), 65–72.

(42) Sousa, M. M.; Berglund, L.; Saraiva, M. J. Transthyretin in high-density lipoproteins: Association with apolipoprotein A-I. *J. Lipid Res.* **2000**, *41* (1), 58–65.

(43) Liz, M. A.; Faro, C. J.; Saraiva, M. J.; Sousa, M. M. Transthyretin, a new cryptic protease. *J. Biol. Chem.* **2004**, *279* (20), 21431–8.

(44) Lee, M.; Kovanen, P. T.; Tedeschi, G.; Oungre, E.; Franceschini, G.; Calabresi, L. Apolipoprotein composition and particle size affect HDL degradation by chymase: Effect on cellular cholesterol efflux. *J. Lipid Res.* **2003**, *44* (3), 539–46.

(45) Liz, M. A.; Gomes, C. M.; Saraiva, M. J.; Sousa, M. M. ApoA-I cleaved by transthyretin has reduced ability to promote cholesterol efflux and increased amyloidogenicity. *J. Lipid Res.* **2007**, *48* (11), 2385−95.

(46) Boucher, J.; Ramsamy, T. A.; Braschi, S.; Sahoo, D.; Neville, T. A.; Sparks, D. L. Apolipoprotein A-II regulates HDL stability and affects hepatic lipase association and activity. *J. Lipid Res.* **2004**, *45* (5), 849−58.

(47) Duverger, N.; Murry-Brelier, A.; Latta, M.; Reboul, S.; Castro, G.; Mayaux, J. F.; Fruchart, J. C.; Taylor, J. M.; Steinmetz, A.; Denefle, P. Functional characterization of human recombinant apolipoprotein AIV produced in *Escherichia coli*. *Eur. J. Biochem.* **1991**, *201* (2), 373−83.

(48) de Haan, W.; Out, R.; Berbee, J. F.; van der Hoogt, C. C.; van Dijk, K. W.; van Berkel, T. J.; Romijn, J. A.; Jukema, J. W.; Havekes, L. M.; Rensen, P. C. Apolipoprotein CI inhibits scavenger receptor BI and increases plasma HDL levels in vivo. *Biochem. Biophys. Res. Commun.* **2008**, *377* (4), 1294−8.

(49) Gordon, S.; Li, H.; Zhu, X.; Shah, A.; Lu, L. J.; Davidson, W. S. A comparison of the mouse and human lipoproteome: Suitability of the mouse model for studies of human lipoproteins. *J. Proteome Res.* **2015**, *14* (6), 2686−95.

(50) Camus, M. C.; Chapman, M. J.; Forgez, P.; Laplaud, P. M. Distribution and characterization of the serum lipoproteins and apoproteins in the mouse, *Mus musculus*. *J. Lipid Res.* **1983**, *24* (9), 1210−28.

(51) Al-Sarraf, A.; Al-Ghofaili, K.; Sullivan, D. R.; Wasan, K. M.; Hegele, R.; Frohlich, J. Complete Apo AI deficiency in an Iraqi Mandaean family: Case studies and review of the literature. *J. Clin. Lipidol.* **2010**, *4* (5), 420−6.

(52) Huang, Y.; Wu, Z.; Riwanto, M.; Gao, S.; Levison, B. S.; Gu, X.; Fu, X.; Wagner, M. A.; Besler, C.; Gerstenecker, G.; Zhang, R.; Li, X. M.; DiDonato, A. J.; Gogonea, V.; Tang, W. H.; Smith, J. D.; Plow, E. F.; Fox, P. L.; Shih, D. M.; Lusis, A. J.; Fisher, E. A.; DiDonato, J. A.; Landmesser, U.; Hazen, S. L. Myeloperoxidase, paraoxonase-1, and HDL form a functional ternary complex. *J. Clin. Invest.* **2013**, *123* (9), 3815−28.

(53) Phillips, M. C. New insights into the determination of HDL structure by apolipoproteins: Thematic review series: high density lipoprotein structure, function, and metabolism. *J. Lipid Res.* **2013**, *54* (8), 2034−48.